Activation of Surface Hydroxyl Groups by Modification of H-Terminated Si(111) Surfaces

Peter Thissen,*,[†] Tatiana Peixoto,[†] Roberto C. Longo,[†] Weina Peng,[†] Wolf Gero Schmidt,[‡] Kyeongjae Cho,[†] and Yves J. Chabal[†]

[†]Department of Materials Science and Engineering, University of Texas at Dallas, 800 West Campbell Road, Richardson, Texas 75080, United States

[‡]Lehrstuhl für Theoretische Physik, Universität Paderborn, 33098 Paderborn, Germany

Ⓢ *Supporting Information*

ABSTRACT: Chemical functionalization of semiconductor surfaces, particularly silicon oxide, has enabled many technologically important applications (e.g., sensing, photovoltaics, and catalysis). For such processes, hydroxyl groups terminating the oxide surface constitute the primary reaction sites. However, their reactivity is often poor, hindering technologically important processes, such as surface phosphonation requiring a lengthy postprocessing annealing step at 140 °C with poor control of the bonding geometry. Using a novel oxide-free surface featuring a well-defined nanopatterned OH coverage, we demonstrate that hydroxyl groups on oxide-free silicon are more reactive than on silicon oxide. On this model surface, we show that a perfectly ordered layer of monodentate phosphonic acid molecules is chemically grafted *at room temperature*, and explain why it remains completely stable in aqueous environments, in contrast to phosphonates grafted on silicon oxides. This fundamental understanding of chemical activity and surface stability suggests new directions to functionalize silicon for sensors, photovoltaic devices, and nanoelectronics.
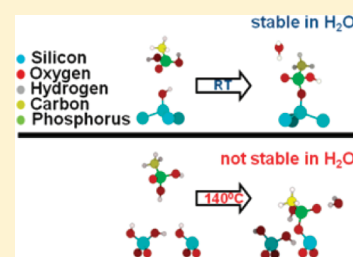
INTRODUCTION

Biomedical, energy, surface coating and protection, and sensor applications all require selective organic surface functionalization of inorganic, electronically active substrates such as silicon.[1−3] The exceptionally good electrical properties of Si/SiO$_2$ interfaces and the use of glass substrates have focused attention and effort on grafting molecules via hydroxyl groups that typically terminate SiO$_2$ surfaces after wet chemical cleaning. However, activation is difficult for some important molecules, such as phosphonates, and therefore constitutes a roadblock for further development of a large number of devices.

Phosphonates are of particular interest for their use in coatings, sensors, electronics, and adhesive promoters[4−7] and have been successfully grafted on metal oxides, for metals such as aluminum, magnesium, titanium, silicon, iron, zinc, nickel, silver, tantalum, and more specific alloys such as stainless steel, AZ31, SS316L, and Nitinol.[5,8−13] The possibility to deposit phosphonates in an ambient environment (i.e., in the presence of water vapor) makes them attractive for low cost processing.[14]

The problem arises in the grafting of phosphonates of silicon oxide. Under normal ambient conditions, phosphonate molecules do not react chemically on silicon oxide or even TiO$_2$. For instance, Gawalt et al. discovered that the adhesion and stability of phosphonic acid SAMs on TiO$_2$ require thermal annealing after deposition of a thin phosphonic acid film. Without this annealing step, it was proposed that the phosphonic acid molecules in the as-deposited film are simply H-bonded to the substrate and among themselves. The molecule−molecule interactions (van der Waals and H-bonding) are apparently stronger than substrate−molecule interactions in the deposited films. Thermal energy derived from annealing fosters covalent attachment of the phosphonic acids to the substrate.[15] Hanson et al. built on this success to formulate a new technique for grafting phosphonic acid films, referred to as the tethering by aggregation and growth (T-BAG) method.[16] While this method leads to chemisorption, the quality of the films is not sufficient to derive the bonding mechanism or to prevent degradation in aqueous solutions. Indeed, in contrast to most of the metal−phosphonic acid bonds, the Si−O−P on the SiO$_x$ bond is sensitive toward hydrolysis.[17] Therefore, the poor reactivity of OH-terminated SiO$_x$ surfaces (preventing ambient grafting) coupled with the vulnerability of the Si−O−P bonds once formed (by annealing) constitute a roadblock that has remained unsolved for over a decade.

Here, we demonstrate that hydroxyl groups terminating an otherwise *oxide-free* (H-terminated) Si(111) surface present all the attributes required for the proposed applications, namely sufficient reactivity for room-temperature grafting of phosphonate molecules, high electrical quality (low density of electronic interface traps), and remarkable stability of phosphonate molecules (Si−O−P bond) in aqueous solutions. Using an oxide-free OH-terminated Si(111) surface,[18] we experimentally show and theoretically confirm that OH on Si(111) (Si$_3$−Si−OH) is more reactive than OH on silicon oxide (O$_3$−Si−OH). We further show that phosphonic acids are chemically attached to the surface as a monodentate via a Si−O−P bond,

with the remaining groups (P=O and P—OH) forming an oriented 2D-network of H-bonds that greatly stabilizes the surface in aqueous solutions. The perfection of the surface (that remains atomically flat throughout the modification) imparts its remarkable properties, highlighting the importance of *oxide-free* surfaces, and makes it possible to model both reactivity and stability using first principle calculations. These findings provide a novel pathway to develop methods for organic modifications of oxide-free surfaces.

■ EXPERIMENTAL METHODS

Anhydrous methanol (CH_3OH, 99.8%), methylphosphonic acid (MPA, $CH_3PO_3H_2$, 99.8%), and octadecylphosphonic acid (ODPA, $CH_3[CH_2]_{17}PO_3H_2$, 99.8%) were purchased from Aldrich. These chemicals, used as received, were placed inside a $N_2(g)$-purged glovebox prior to use. Aqueous ammonium fluoride (40 wt %) and aqueous hydrofluoric acid (49 wt %) were obtained from J.T. Baker. Aqueous hydrogen peroxide (30 wt %) and concentrated (18 M) sulfuric acid were obtained from Fisher Scientific. All H_2O is deionized with a resistivity of 18.2 MΩ cm.

N-type (phosphorus-doped, resistivity of 24–34 Ω cm) float-zone Si(111) wafers, polished on both sides, were cut into 1.5 cm ×3.8 cm pieces for infrared transmission measurements. Oxides were chemically cleaned by 30 min of exposure to an 80 °C solution of 3:1 concentrated (18 M) H_2SO_4/30% H_2O_2(aq) (hereafter referred to as piranha solution) to remove organic contamination. Si(111) samples were hydrogen terminated by a 30 s dip in 10–20% HF(aq) followed by a 2.5 min dip in 40% NH_4F(aq), and a final rinse in H_2O for 10 s.[19] This latter procedure produces an atomically smooth (111)-oriented surface for tens to hundreds of nanometers. Silicon samples of (111)-orientation were often reused since an atomically flat surface could be prepared between subsequent experiments.

FTIR data were recorded in the dry $N_2(g)$-purged bench of a Fourier transform infrared (FTIR) spectrometer (Nicolet 6700). Spectra were obtained with a nominal 4 cm^{-1} resolution between 400 and 4000 cm^{-1} in transmission mode, at an angle of incidence of 64° with respect to the Si surface normal. A room temperature pyroelectric detector (DTGS) was used for data collection. Five consecutive loops, each consisting of 1000 single beam spectral scans, were obtained for each sample. References were either oxide terminated or freshly etched hydrogen terminated surfaces, as appropriate.

XPS analysis was performed with a Quantum 2000 Scanning ESCA Microprobe (Physical Electronics, USA) spectrometer equipped with a concentric hemispherical analyzer under ultrahigh vacuum conditions (10^{-9} mbar) and an Al $K_α$ X-ray source (15 keV, filament current 20 mA). Spectra were recorded at a 45° takeoff angle with respect to the surface. A sample area of 100 μm × 100 μm was analyzed with a pass energy of 46.95 eV for survey and 11.75 eV for detailed elemental scans. The spectra obtained were analyzed using CASA XPS software, surface sensitivity factors used to determine the atomic concentration were taken from the MultiPak Version 6.0 software (supplied by Physical Electronics).

The calculations were performed using DFT within the generalized gradient approximation (GGA) as implemented in the Vienna ab initio simulation package (VASP). The electron−ion interaction was described by the projector-augmented wave scheme. The electronic wave functions were expanded into plane waves up to a kinetic energy of 360 eV. The surface was modeled by periodically repeated slabs. The supercell used here consisted of 8 atomic layers of Si plus adsorbed molecules and a vacuum region equivalent to 16 atomic layers. The 7 uppermost layers of Si as well as the adsorbate degrees of freedom were allowed to relax until the forces on the atoms are below 10 meV/Å. The Brillouin zone integration was performed using 4 × 4 × 1 mesh within the Monkhorst−Pack scheme. The PW91 functional was used to describe the electron exchange and correlation energy within the GGA.[20−22] Eigenmodes were calculated by the force-constant (FC) approach, diagonalizing the mass weighted second derivative matrix (Hessian) in the case of the adsorbed species and the

top Si layer. The restriction to the atoms of the top layer and the adsorbed species is legitimate because the eigenmodes of these atoms do not overlap with the eigenmodes of the bulk material. Kinetic barriers were calculated by the nudged elastic band (NEB) method, using a string of geometric configurations to describe the reaction pathway of the system. A spring interaction between every configuration ensured continuity of the reaction pathway.

■ RESULTS AND DISCUSSION

An atomically flat, hydrogen-terminated Si(111) surface is used as the starting point for the surface modifications in wet chemical experiments. The sample is first immersed in anhydrous methanol at 65 °C for 12 h, followed by immersion in HF(aq) (49 wt %) for 3 min, replacing the Si−OCH_3 bond and forming a Si−F bond.[23] Next, exposure of the F-terminated surface to pure water for 90 s results in a 1/3 ML OH and 2/3 ML H-terminated Si(111) surface (see Supporting Information for IR and XPS data of every reaction step).[18] This atomically flat surface, characterized by Si−OH groups surrounded by six Si−H units, ensures that the OH groups are too far (∼3.9 Å) to be hydrogen bonded.

When immersed in a methylphosphonic acid (MPA) solution (conc. 10^{-3} mol/L in methanol, time ∼12 h) at room temperature,[18,23−25] the OH groups clearly react. The differential infrared absorption spectrum (Figure 1), measured
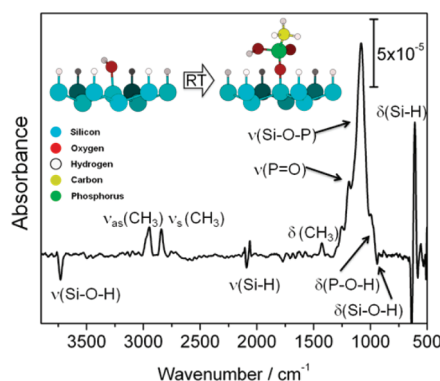

Figure 1. Differential infrared absorption spectrum: Transmission spectrum taken after the reaction with MPA (shown in inlet graph), referenced to the initial hydroxylated surface.

before and after this last reaction step, shows a loss of the SiOH stretch (3730 cm^{-1}) and Si−O−H deformation (∼800 cm^{-1}) modes, confirming the condensation reaction of SiOH with the MPA.[26,27] Associated with the disappearance of the SiOH eigenmodes, two other features confirm the chemisorption reaction. First, the stretch and umbrella CH_3 modes associated with the MPA are clearly visible at ν_{as} = 2947 cm^{-1} and ν_s = 2840 cm^{-1} and δ = 1427 cm^{-1}. Second, the Si−H stretch and bending modes are perturbed, exhibiting a red shift from ν = 2083 cm^{-1} to 2081 cm^{-1}, and from δ = 626 cm^{-1} to 620 cm^{-1}, respectively, without any loss of their total integrated areas. These observations are consistent with chemical grafting of the MPA molecules at the surface hydroxyl groups, with no hydrogen removal, oxidation, or roughening of the surface.

The unambiguous proof of chemisorption comes from examination of the 800−1400 cm^{-1} spectral region. There is a clear and strong contribution corresponding to the Si−O−P stretch mode at 1080 cm^{-1}, which has been previously observed upon chemical reaction of phosphonate molecules with silicon oxide resulting from the phosphonic acid condensation reaction

with SiOH.[16,28] Furthermore, the shoulders at 1160 and 940 cm^{-1} can be assigned to the P=O stretch mode and the P—O—H deformation mode of the MPA molecule,[28] providing strong evidence for monodentate chemisorption. Therefore, adsorption on this model surface differs from the bidentate and the tridentate bonding seen in other phosphonate/oxide systems,[4,5,8,11,14,16,28−30] primarily because of the separation between the hydroxyl groups (3.9 Å).

While the IR absorption spectrum provides evidence for chemisorption in the monodentate configuration, it is difficult to know if the silicon surface remains unoxidized because the SiO$_2$ phonon modes occur in the 1000−1250 cm^{-1} region,[24] overlapping the Si—O—P and associated oxygen vibrations. Therefore, complementary X-ray photoelectron spectroscopy (XPS) measurements were performed at each step of the surface modification. Figure 2 of the Si 2p core level spectra
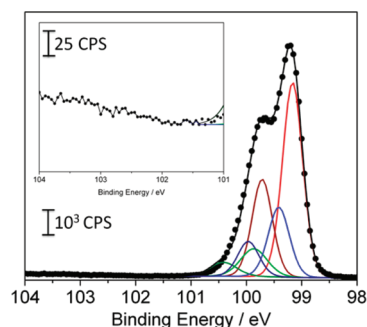

Figure 2. X-ray photoelectron spectrum of the Si 2p region. Detail spectrum of the 1/3 ML OH and 2/3 ML H-terminated Si(111) surface. The inset is a ×40 expanded region to show the absence of any contribution from Si oxidation states +2, +3, and +4. Color scheme of the fitting: red, Si 2p$_{3/2}$^{bulk}; wine, Si 2p$_{1/2}$^{bulk}; blue, Si 2p$_{3/2}$^{hydrogen}; navy, Si 2p$_{1/2}$^{hydrogen}; green, Si 2p$_{3/2}$^{MPA}; olive, Si 2p$_{1/2}$^{MPA}.

reveals that there is no contribution in the 101−104 eV range (see inset), from oxidation states higher than +1 for Si, i.e. any type of oxide,[27] despite exposure to air prior to the measurement. The spectrum itself is then fitted for Si—O (+0.9 eV for +1 oxidation state) and Si—H (+0.25 eV, using values from the literature).[31,32] With this fitting, we find that

the Si—H component decreases by 33% ± 1% from its value for a fully H-terminated Si(111) surface, and the Si—O component involves 33% ± 1% ML of surface Si atoms (see Supporting Information). The XPS data establish therefore that the surface remains oxide free.

The reactivity of the 1/3 ML OH and 2/3 ML H-terminated Si(111) surface is clearly much higher than oxidized silicon surfaces. This surprising finding can be understood with first-principles calculations. Figure 3 displays the energy barriers obtained from density functional theory (DFT) that are associated with the transition states for the adsorption process of MPA on a model oxide surface, namely on the fully and partially hydroxylated SiO$_2$(100) and on the 1/3 ML OH and 2/3 ML H-terminated Si(111) surfaces. For MPA chemisorption, the barrier is ~1.3 eV on the fully hydroxylated SiO$_2$(100) surface, consistent with the required 140 °C T-BAG procedure. In contrast, the barrier is reduced to ~1.1 eV for the partially hydroxylated and ~0.9 eV for the oxide-free 1/3 ML OH and 2/3 ML H-terminated Si(111) surface, consistent with reaction at room temperature on the latter when solvation effects are included.

The origin of this difference is subtle and less related to the strength of the Si—OH bond and more to the stabilization of the initial hydroxyl groups on oxide surfaces. Figure 3 illustrates that, despite a similar reaction pathway, the MPA molecule is required to deform to connect the P and O atoms at the transition state, due to the initial hydrogen bonding of the OH groups on the fully hydroxylated oxide, adding +0.3 eV to the barrier. In addition, there is less charge transfer for OH groups on SiO$_2$ (oxidation state = +4) than on oxide-free silicon (oxidation state = +1), adding +0.15 eV to the barrier. Overall, the oxide-free surface is more reactive by 0.45 eV.

DFT calculations also indicate that the monodentate configuration is the only chemisorption geometry possible for MPA adsorption on this oxide-free OH-terminated Si(111) surface. The energy associated with a bi- and tridentate is substantially higher due to large strains needed to link three OH centers separated by 3.9 Å to the oxygen atoms of the phosphonic acid head separated by 2.3 Å (see Figure S5). In the monodentate configuration, the P—OH and P=O groups are found to lock into a well-defined pattern, as illustrated in
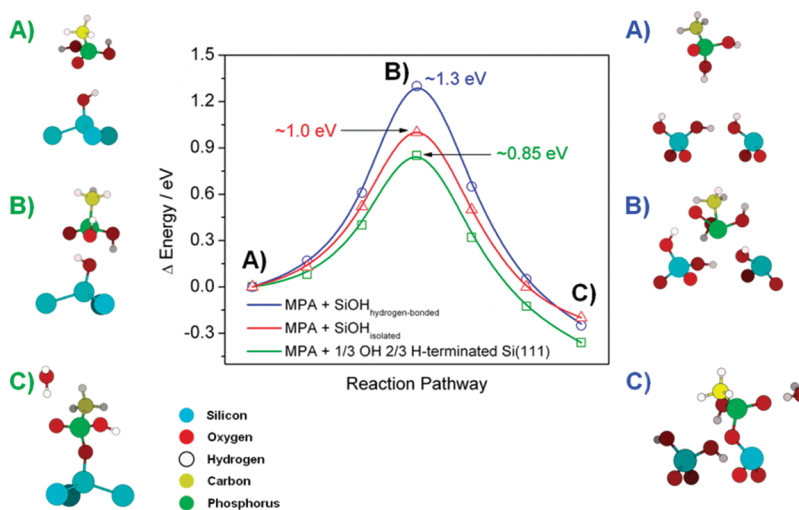

Figure 3. Reaction pathways for MPA reacting with 1/3 ML OH and 2/3 ML H-terminated Si(111) surface (green line) and MPA reacting with OH-terminated SiO$_2$(100) (blue line). The red line corresponds to MPA reacting with an isolated OH group on SiO$_2$(100).

Figure S5 of the Supporting Information. This bonding configuration at the interface is also found for longer chain phosphonates, confirming that the chain length does not influence the overall process.

The stability of the monodentate bond 1/3 ML MPA and 2/3 ML H-terminated Si(111) surface appears questionable from a thermodynamic point of view compared to bi- and tridentates.[29] An unstable surface would suffer hydrolysis removal of phosphonates with subsequent oxidation of the Si surface. We have therefore examined the stability of this surface after substantial (30 min) water immersion with XPS. The Si 2p core level spectrum (see Table S1) indicates that the surface remains completely oxide free.

The mechanism for such interface stabilization is revealed from infrared absorption spectra of hydrated surfaces and associated DFT calculations. Figure 4 shows the IR differential
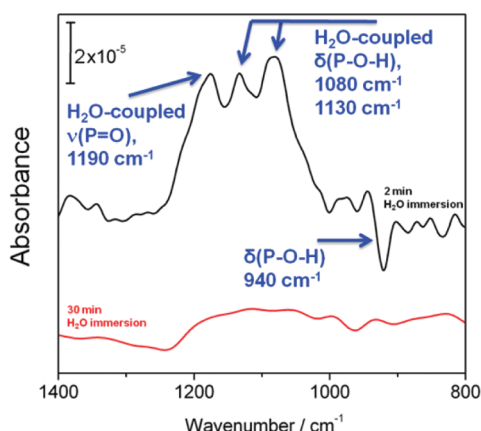

Figure 4. **Infrared spectra of hydrated surface as a function of immersion time**: The top spectrum, referenced to the 1/3 ML MPA and 2/3 ML H-terminated Si(111): 1/3 ML MPA and 2/3 ML H-terminated Si(111) is obtained after 2 min of immersion in water. The bottom, referenced to the top spectrum, shows the *changes* associated with an additional 30 min of immersion.

spectra of the 1/3 ML MPA and 2/3 ML H-terminated Si(111) surface, focusing in the $800-1400$ cm^{-1} spectral region before and after sequential water immersion (initially for 2 min then in intervals of 10 min), with the spectra referenced to the 1/3 ML MPA and 2/3 ML H-terminated Si(111) surface. There is a clear loss of P—O—H deformation mode at 940 cm^{-1} and a corresponding gain at 1130 and 1080 cm^{-1}. In addition, the P=O stretch mode at 1190 cm^{-1} is strengthened. An extensive search of possible geometries using DFT calculations reveals that H_2O molecules are incorporated within the near surface region in the vicinity of the phosphorus structures (P=O, P—O—H) in two different ways. As illustrated in Figure 5 and quantified in Table 1, H_2O is either H-bonded through its oxygen to the hydrogen of P—OH (water is an acceptor as shown in red highlight in Figure 5) or through its hydrogen to the oxygen of P—OH (water is a donor as shown in green highlight in Figure 5). These two configurations lead to two P—O—H deformation modes at 1130 and 1080 cm^{-1}, respectively, which are both blue-shifted compared to the free P—OH mode at 940 cm^{-1}. The relative strengthening of the P=O stretch and these two P—O—H deformation modes is consistent with H-bonding to H_2O molecules. Individual H-bond analysis via electron density allows the quantification of contribution to intermolecular interactions.[33] We find that the
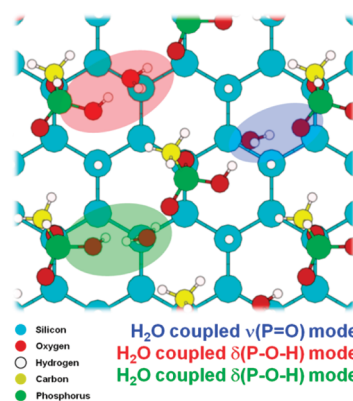

Figure 5. **Location of water molecules in MPA layer**. Top view of 1/3 ML MPA and 2/3 ML H-terminated Si(111) surface with position of water molecules calculated to be in bridge positions.

H-bonds are ~1.8 Å long and stabilize the structures by an energy of ~0.7 eV per H-bond, i.e. ~1.4 eV per phosphonate group.

Importantly, the two-dimensional network of H-bonds, involving the P=O, P—OH, and H_2O, provides the necessary rigidity and steric barrier to prevent substrate oxidation. First, all the surface species are tightly H-bonded through water incorporation as quantified above. Second, the location of the tightly H-bonded water molecules prevents access to the Si—O—P bond necessary for hydrolysis, hence the stability of the silicon/adsorbate interface.

A powerful method to examine the incorporation of a polar molecule within an organic layer such as MPA is spectroscopic ellipsometry because any such incorporation leads to a notable increase of the index of refraction without a change in layer thickness. We therefore performed spectroscopic ellipsometric measurements on 1/3 ML MPA and 2/3 ML H-terminated Si(111) surfaces and also on H-terminated Si(111) surfaces after immersion in water for comparison. As detailed in the Supporting Information, the results show a clear increase of the refraction index from 1.15 to 1.44 (see Table S3), without swelling (thickness increase) of the layer. These results strongly support the incorporation of only the H_2O participating in the H-bonded surface network. Importantly, the spectroscopic ellipsometric spectra are all fitted without requiring a silicon oxide layer, in agreement with IR and XPS data.

The stability of the 1/3 ML MPA and 2/3 ML H-terminated Si(111) surfaces was further tested in harsh wet chemical environments, such as acidic solutions. Good resistance was observed at acidic pH values (e.g., in HF, pH ~1). This finding is not completely unexpected because of the acidic nature of the phosphonic acid free molecules (pK_a ~3)[34] but is important for sensing applications.

In general, the stability of long chain SAMs has been understood in the past by the reduction in interface ion transport. For the MPA we are now able to show a new mechanism for the stability of phosphonic acids. Water molecules can be trapped between phosphonic acid molecules at the 1/3 ML MPA and 2/3 ML H-terminated Si(111), providing a barrier for substrate oxidation. Importantly, the presence of these water molecules does not affect the electronic quality of the *silicon/SAM* interface, as confirmed by photoluminescence measurements (Supporting Information, Figure S7). In comparison to purely H-terminated Si(111) surfaces,

Table 1. Experimentally Found and DFT Calculated Wavenumbers with Assigned Eigenmodes

eigenmode	frequency/cm^{-1}		eigenmode	frequency/cm^{-1}	
1/3 ML MPA 2/3 ML H-terminated Si(111)	experimentally found	DFT calculated	1/3 ML MPA 2/3 ML H-terminated Si(111) + H$_2$O	experimentally found	DFT calculated
ν(P=O)	1160–1190	1160–1170	ν(P=O) + H$_2$O	1160–1190	1210–1230
δ(P–O–H)	940	960–970	δ(P–O–H) + H$_2$O	1130, red area in Figure 5 1080, green area in Figure 5	1130–1100, red area in Figure 5 1030–1070, green area in Figure 5

the 1/3 ML MPA, 2/3 ML H-terminated Si(111) surfaces maintain their photoluminescence yield for long times (≫ 5 h).

The stability of the *SAM top* interface (i.e., SAM/air interface) is best probed by contact angle measurements. As detailed in the Supporting Information (Figure S3), we find that the 1/3 ML MPA and 2/3 ML H-terminated Si(111) surfaces are characterized by a static contact angle (CA) of ∼80° that remains stable over weeks. This confirms the hydrophobic nature of the methyl group and underscores the high stability of these surfaces compared to H-terminated Si(111) surfaces.

To examine the whole system, including bottom Si/SAM and top SAM/air interfaces, current–voltage (I–V) measurements have been performed using a mercury drop for top contact on (i) 1/3 ML MPA and 2/3 ML H-terminated Si(111), (ii) 1/3 ML octadecylphosphonic acid (ODPA) and 2/3 ML H-terminated Si(111), and (iii) H-terminated Si(111) surfaces. For H-terminated Si(111) surfaces, with no detectable surface dangling bonds and negligible band bending, the I–V curve is a straight line passing through the origin (see Figure S8). This ohmic-like behavior is consistent with a very thin Si–H (1.49 Å thick) interface.[35] In contrast, an obvious rectifying behavior is observed for both Si-ODPA- and Si-MPA-terminated surfaces, indicating the presence of a Schottky barrier at the Si surface for short and long chain phosphonates. Because of the organic barrier, the molecule/Si junction behaves like a diode that conducts at forward bias and passes very low current under reverse bias. The tunneling current is dominated by thermionic emission through the barrier and also includes a tunneling component through the molecule layers, which can be measured by using two different chain-length phosphonate molecules. There is no observable dependence on chain length at higher forward bias which is most likely due to the series resistance in the system. This resistance arises from the 1/3 monolayer density of Si–O–P bonds through which the current passes.[36] The strong rectification between the MPA and ODPA termination shows that the transport across these junctions is not dominated by defects.[35]

Interestingly, the surface electrical behavior appears to be completely dominated by the grafted molecule even though the surface only has 1/3 ML of MPA species and the rest of the Si atoms are still hydrogen terminated. This confirms the importance of the phosphonate group on the interface properties. The exact barrier height is strongly affected by the Si-molecule interaction, e.g., the charge transfer between the molecule and Si, in addition to the molecule dipole and interface states. From our experiments we estimate a charge transfer of ∼1e from silicon atoms connected in the monodentate configuration to the oxygen of the MPA. Performing Bader charge analysis,[37] we find that a charge of 1.012e is transferred to the O directly from the Si atoms to which they are bonded, while subsurface atoms remain almost unaffected. This charge transfer beautifully agrees with the Si 2p

core level shift and is responsible for an additional band bending. Therefore, the nanopatterned Si surface can serve as a template with minimal influences on the overall electrical behavior, making it possible *to probe the charge transfer associated with the adsorbate only*.

◼ CONCLUSION

In summary, the synthesis of a novel model system has provided insight into the nature of surface hydroxyl groups. Hydrogen bonding and to a lesser extent the oxidation state of the surface Si atom stabilize OH-terminated silicon oxide surfaces, rendering them unfavorable for phosphonate chemisorption. In contrast, phosphonic acid molecules can be grafted on oxide-free silicon at room temperature in a monodentate configuration. This work has also provided fundamental insight into the role of water molecules in preventing hydrolysis of phosphonated surfaces. Finally, the fundamental electrical parameters of these silicon/SAM interfaces have been measured, such as the charge transfer at this interface. In general, a detailed structure for the phosphonic acids has been derived on an atomic level and can be used as a guide for characterization in future work and for a host of applications.

◼ ASSOCIATED CONTENT

⑤ Supporting Information

Infrared, XPS, contact angle, DFT, photoluminescence, electrical properties, ellipsometry. This material is available free of charge via the Internet at http://pubs.acs.org.

◼ AUTHOR INFORMATION

Corresponding Author

peter.thissen@utdallas.edu

Notes

The authors declare no competing financial interest.

◼ ACKNOWLEDGMENTS

◼ REFERENCES

(1) Buriak, J. M. *Chem. Rev.* **2002**, *102*, 1271–1308.
(2) Love, J. C.; Estroff, L. A.; Kriebel, J. K.; Nuzzo, R. G.; Whitesides, G. M. *Chem. Rev.* **2005**, *105*, 1103–1169.
(3) Aswal, D. K.; Lenfant, S.; Guerin, D.; Yakhmi, J. V.; Vuillaume, D. *Anal. Chim. Acta* **2006**, *568*, 84–108.
(4) Dubey, M.; Weidner, T.; Gamble, L. J.; Castner, D. G. *Langmuir* **2010**, *26*, 14747–14754.

(5) Thissen, P.; Wielant, J.; Koeyer, M.; Toews, S.; Grundmeier, G. *Surf. Coat. Technol.* **2010**, *204*, 3578−3584.

(6) Wapner, K.; Stratmann, M.; Grundmeier, G. *Int. J. Adhes. Adhes.* **2008**, *28*, 59−70.

(7) Acton, O.; Hutchins, D.; Arnadottir, L.; Weidner, T.; Cernetic, N.; Ting, G. G.; Kim, T. W.; Castner, D. G.; Ma, H.; Jen, A. K. Y. *Adv. Mater.* **2011**, *23*, 1899−1902.

(8) Giza, M.; Thissen, P.; Grundmeier, G. *Langmuir* **2008**, *24*, 8688−8694.

(9) Maxisch, M.; Thissen, P.; Giza, M.; Grundmeier, G. *Langmuir* **2011**, *27*, 6042−6048.

(10) Quinones, R.; Raman, A.; Gawalt, E. S. *Thin Solid Films* **2008**, *516*, 8774−8781.

(11) Raman, A.; Dubey, M.; Gouzman, I.; Gawalt, E. S. *Langmuir* **2006**, *22*, 6469−6472.

(12) Raman, A.; Quinones, R.; Barriger, L.; Eastman, R.; Parsi, A.; Gawalt, E. S. *Langmuir* **2010**, *26*, 1747−1754.

(13) Zorn, G.; Gotman, I.; Gutmanas, E. Y.; Adadi, R.; Salitra, G.; Sukenik, C. N. *Chem. Mater.* **2005**, *17*, 4218−4226.

(14) Thissen, P.; Valtiner, M.; Grundmeier, G. *Langmuir* **2010**, *26*, 156−164.

(15) Gawalt, E. S.; Avaltroni, M. J.; Koch, N.; Schwartz, J. *Langmuir* **2001**, *17*, 5736−5738.

(16) Hanson, E. L.; Schwartz, J.; Nickel, B.; Koch, N.; Danisman, M. F. *J. Am. Chem. Soc.* **2003**, *125*, 16074−16080.

(17) Guerrero, G.; Mutin, P. H.; Vioux, A. *Chem. Mater.* **2001**, *13*, 4367−4373.

(18) Michalak, D. J.; Amy, S. R.; Aureau, D.; Dai, M.; Esteve, A.; Chabal, Y. J. *Nat. Mater.* **2010**, *9*, 266−271.

(19) Jakob, P.; Chabal, Y. J. *J. Chem. Phys.* **1991**, *95*, 2897−2909.

(20) Kresse, G.; Furthmuller, J. *Comput. Mater. Sci.* **1996**, *6*, 15−50.

(21) Kresse, G.; Furthmuller, J. *Phys. Rev. B* **1996**, *54*, 11169−11186.

(22) Kresse, G.; Joubert, D. *Phys. Rev. B* **1999**, *59*, 1758−1775.

(23) Michalak, D. J.; Rivillon, S.; Chabal, Y. J.; Esteve, A.; Lewis, N. S. *J. Phys. Chem. B* **2006**, *110*, 20426−20434.

(24) Michalak, D. J.; Amy, S. R.; Esteve, A.; Chabal, Y. J. *J. Phys. Chem. C* **2008**, *112*, 11907−11919.

(25) Webb, L. J.; Rivillon, S.; Michalak, D. J.; Chabal, Y. J.; Lewis, N. S. *J. Phys. Chem. B* **2006**, *110*, 7349−7356.

(26) Asay, D. B.; Kim, S. H. *J. Phys. Chem. B* **2005**, *109*, 16760−16763.

(27) Vandervoort, P.; Gillisdhamers, I.; Vansant, E. F. *J. Chem. Soc., Faraday Trans.* **1990**, *86*, 3751−3755.

(28) Quinones, R.; Gawalt, E. S. *Langmuir* **2007**, *23*, 10123−10130.

(29) Luschtinetz, R.; Oliveira, A. F.; Frenzel, J.; Joswig, J.-O.; Seifert, G.; Duarte, H. A. *Surf. Sci.* **2008**, *602*, 1347−1359.

(30) Luschtinetz, R.; Seifert, G.; Jaehne, E.; Adler, H. J. P. *Macromol. Symp.* **2007**, *254*, 248−253.

(31) Himpsel, F. J.; Heimann, P.; Chiang, T. C.; Eastman, D. E. *Phys. Rev. Lett.* **1980**, *45*, 1112−1115.

(32) Himpsel, F. J.; Meyerson, B. S.; McFeely, F. R.; Morar, J. F.; Talebibrahimi, A.; Yarmoff, J. A. In *Photoemission and Absorption Spectroscopy of Solids and Interfaces with Synchrotron Radiation*; Elsevier Science Publishers B.V.: Amsterdam, 1990; Vol. *108*, pp 203−236.

(33) Jones, G.; Jenkins, S. J.; King, D. A. *Surf. Sci.* **2006**, *600*, L224−L228.

(34) Liakos, I. L.; Newman, R. C.; McAlpine, E.; Alexander, M. R. *Langmuir* **2007**, *23*, 995−999.

(35) Vilan, A.; Yaffe, O.; Biller, A.; Salomon, A.; Kahn, A.; Cahen, D. *Adv. Mater.* **2010**, *22*, 140−159.

(36) Yaffe, O.; Scheres, L.; Puniredd, S. R.; Stein, N.; Biller, A.; Lavan, R. H.; Shpaisman, H.; Zuilhof, H.; Haick, H.; Cahen, D.; Vilan, A. *Nano Lett.* **2009**, *9*, 2390−2394.

(37) Bader, R. F. W. *Atoms in Molecules- A Quantum Theory*; Oxford University Press: Oxford, U.K., 1990.

8874

dx.doi.org/10.1021/ja300270w | *J. Am. Chem. Soc.* 2012, 134, 8869−8874